ACS NANO

www.acsnano.org

ARTICLE

Tuning the Fermi Level of Graphene by Two-Dimensional Metals for Raman Detection of Molecules

Na Zhang,[¶] Kunyan Zhang,[¶] Min Zou, Rinu Abraham Maniyara, Timothy Andrew Bowen, Jonathon Ray Schrecengost, Arpit Jain, Da Zhou, Chengye Dong, Zhuohang Yu, He Liu, Noel C. Giebink, Joshua A. Robinson, Wei Hu,* Shengxi Huang,* and Mauricio Terrones*

Cite This: *ACS Nano* 2024, 18, 8876−8884

Read Online

ACCESS | Metrics & More | Article Recommendations | Supporting Information

ABSTRACT: **Graphene-enhanced Raman scattering (GERS) offers great opportunities to achieve optical sensing with a high uniformity and superior molecular selectivity. The GERS mechanism relies on charge transfer between molecules and graphene, which is difficult to manipulate by varying the band alignment between graphene and the molecules. In this work, we synthesized a few atomic layers of metal termed two-dimensional (2D) metal to precisely and deterministically modify the graphene Fermi level. Using copper phthalocyanine (CuPc) as a representative molecule, we demonstrated that tuning the Fermi level can significantly improve the signal enhancement and molecular selectivity of GERS. Specifically, aligning the Fermi level of graphene closer to the highest occupied molecular orbital (HOMO) of CuPc results in a more pronounced Raman enhancement. Density functional theory (DFT) calculations of the charge density distribution reproduce the enhanced charge transfer between CuPc molecules and graphene with a modulated Fermi level. Extending our investigation to other molecules such as rhodamine 6G, rhodamine B, crystal violet, and F_{16}CuPc, we showed that 2D metals enabled Fermi level tuning, thus improving GERS detection for molecules and contributing to an enhanced molecular selectivity. This underscores the potential of utilizing 2D metals for the precise control and optimization of GERS applications, which will benefit the development of highly sensitive, specific, and reliable sensors.**

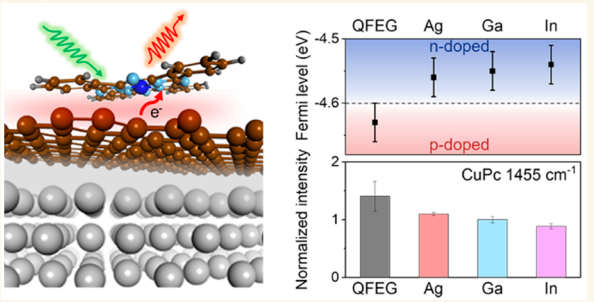

KEYWORDS: *two-dimensional metals, epitaxial graphene, modulation doping, Fermi level tuning, Surface-enhanced Raman scattering, Graphene-enhanced Raman scattering*

INTRODUCTION

Surface-enhanced Raman spectroscopy (SERS) has garnered significant interest in the scientific community over the past decade, as it enables an enhanced detection of molecules, proteins, and biological samples.[1−3] SERS substrates based on metal nanostructures are often limited by their rough and chemically active metal surface, which leads to undesired effects such as photochemical reactions, strong fluorescence background, and nonuniform absorption of probe molecules.[4,5] These factors compromise the reliability, repeatability, and quantifiability of Raman signals and limit the potential applications in the development of integrated and label-free sensors.[6,7] On the other hand, graphene, an ultraflat and chemically inert two-dimensional (2D) material, addresses these drawbacks of traditional SERS substrates by providing uniform and stable enhancement of Raman signals in a phenomenon termed graphene-enhanced Raman scattering (GERS).[8−11] Metal-free GERS has great potential for practical sensing applications that benefit from its excellent chemical stability, uniformity, fluorescence quenching capability, and biocompatibility.[12−14]

The mechanism of GERS is the charge transfer and dipole−dipole interaction between the analyte molecule and graphene, which effectively increases the polarizability change of the molecules and enhancement of the Raman signals.[15,16] Such a charge transfer process is highly dependent on the band alignment between graphene and analyte molecules.[17] There-

Received: December 4, 2023
Revised: March 6, 2024
Accepted: March 12, 2024
Published: March 18, 2024

https://doi.org/10.1021/acsnano.3c12152
ACS Nano 2024, 18, 8876−8884

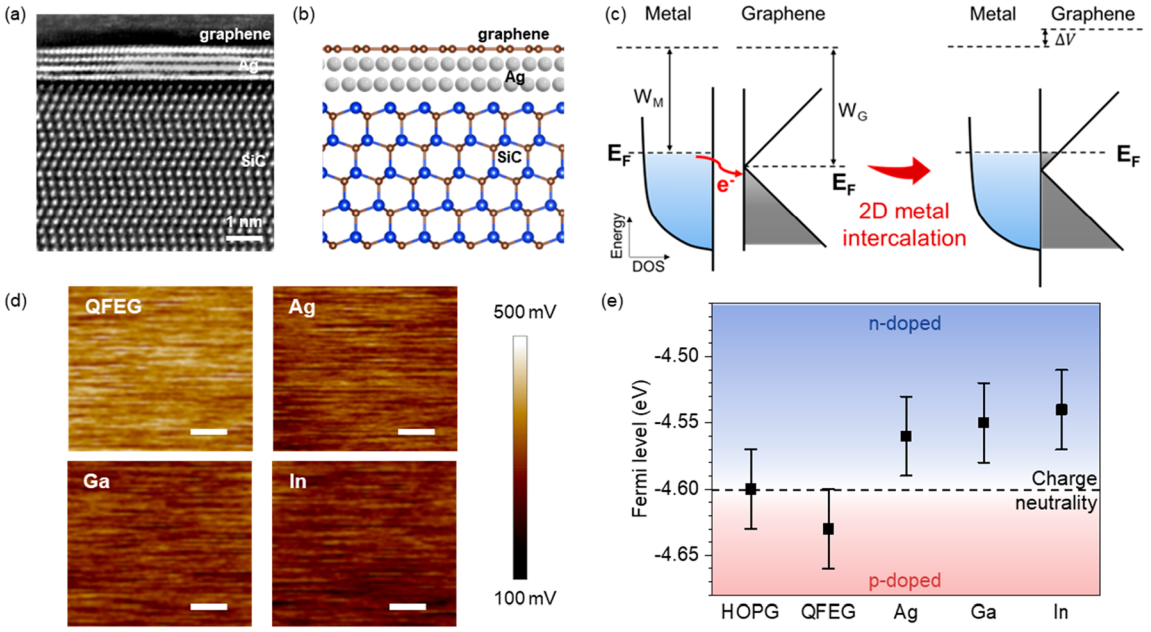

Figure 1. Modulation doping of graphene by 2D metal. (a) STEM image and (b) schematic illustration of 2D metal. (c) Schematic illustration of the Fermi level tuning after graphene is in contact with the metal layer. (d) KPFM mapping of QFEG, 2D Ag, 2D Ga, and 2D In, respectively. The scale bar is 500 nm. (e) Fermi level of different types of graphene obtained from the KPFM mapping image.

fore, tuning the Fermi level of graphene can effectively modulate the degree of charge transfer and provide a better understanding of the transfer pathways related to the enhancement. Various strategies have been applied to tune the Fermi level of graphene, such as applied electric field, electrochemical doping, ultraviolet (UV) radiation, and chemical doping.[18] Although doping by an external electric field is highly controllable, this involves a tedious fabrication process and might introduce undesired contamination.[19,20] Similarly, electrochemical doping is efficient in modulating the Fermi level but requires the introduction of guest molecules with electron-withdrawing or electron-donating groups, which can interfere with the Raman signals of probe molecules.[21] UV radiation only has limited control over doping level and undermines the stability of graphene.[22] When compared with the aforementioned methods, chemical doping provides strong and controllable modulation of the doping level and can be categorized as covalent or noncovalent interaction.[23−26] The covalent interaction involves heteroatoms substituted or covalently bonded to the carbon atoms of graphene; however, it essentially alters the electronic structure of graphene.[27] On the other hand, noncovalent interactions, such as molecular deposition and substrate effects, preserve the electronic structure of graphene.[28] In addition, noncovalent chemical doping can deterministically modulate the Fermi level of graphene, which allows us to probe the correlation between band alignment, charge transfer, and the GERS enhancement without ambiguity.

In this work, we utilized a few layers of metal atoms (2D metals) as an alternative means of chemical doping to fine-tune the Fermi level of graphene and investigated the charge transfer process in GERS. The 2D metal intercalated between the graphene overlayer and the SiC substrate via confinement heteroepitaxy (CHet) forms a graphene/metal/SiC structure (Figure 1a). In this case, metal atoms interact with the graphene through van der Waals forces while covalently bonded to the underlying SiC substrate with strong internal gradients in their bonding character.[29,30] The Fermi surface of 2D metals comes close to the Dirac point of graphene, which benefits the Fermi level modulation of graphene. By intercalating different 2D metals, such as Ag, Ga, and In, at the graphene/SiC interface, we demonstrated that the Fermi level of the graphene can be delicately tuned, as shown by Kelvin probe force microscopy (KPFM). Using copper phthalocyanine (CuPc) as a model molecule, we demonstrated that Fermi level tuning can change the GERS performance. More specifically, a stronger Raman enhancement was observed when aligning the Fermi level of graphene closer to the highest occupied molecular orbital (HOMO) level of CuPc. This effect is attributed to enhanced binding and charge transfer between CuPc molecules and graphene, as supported by density functional theory (DFT) calculations. Further studies of different molecules with varied band alignment with graphene, including rhodamine 6G (R6G), rhodamine B (RhB), crystal violet (CV), and F_{16}CuPc, confirmed that the Fermi level tuning based on 2D metals can improve the GERS effect through a better band alignment, which in turn provides the possibility to selectively enhance the Raman signals of molecules through band alignment.

RESULTS AND DISCUSSION

Fermi Level Tuning by 2D Metals. The graphene/Ag/SiC (labeled as 2D Ag for simplicity) was synthesized by intercalating metal atoms underneath the epitaxial graphene layer on SiC. The cross section of 2D Ag was characterized using high-resolution, high angle annular dark-field scanning transmission electron microscopy (HAADF-STEM) as shown in Figure 1a. Figure 1b depicts the 2D Ag where a few layers of silver atoms are intercalated between graphene and the SiC (0001) substrate. The corresponding scanning electron microscopy (SEM) and atomic force microscopy (AFM) images confirm the intercalation of Ag (Figure S1, S2). X-ray

https://doi.org/10.1021/acsnano.3c12152
ACS Nano 2024, 18, 8876−8884

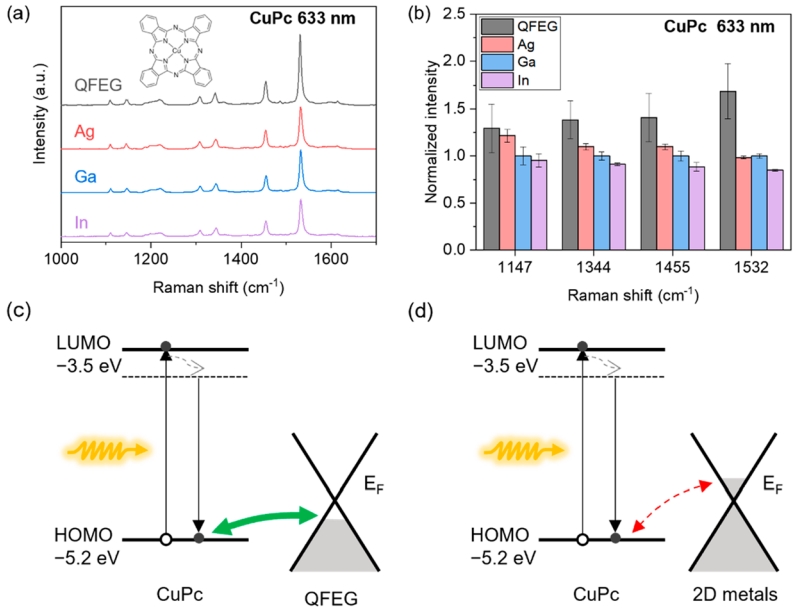

Figure 2. Raman enhancement of CuPc on 2D metals and QFEG. (a) Raman spectra of CuPc on QFEG, 2D Ag, 2D Ga, and 2D In under 633 nm excitation. (b) Intensity of the Raman modes of CuPc normalized by 2D Ga. The error bars represent the standard deviations of multiple measurements. Schematic band alignment and charge transfer between CuPc and graphene for (c) QFEG and (d) 2D metals.

photoelectron spectroscopy (XPS) studies also suggest the successful intercalation of 2D metals by observing the shift of the C 1s peak attributed to SiC (Figure S3). The modulation of the graphene Fermi level by the underlying 2D metals is illustrated in Figure 1c. Graphene is a semimetal with a linear dispersion relation at the Dirac point. Once graphene is in contact with 2D metals, electron transfer occurs between the metal and graphene until the Fermi levels are aligned, resulting in the doping of graphene. Quasi-free-standing epitaxial graphene (QFEG), which is obtained on SiC by hydrogen intercalation (Figure S4a), was also included in this study to provide an efficient hole doping of graphene.[30]

To confirm the electron doping and Fermi level tuning of graphene depicted here, we performed a KPFM measurement on graphene with different types of 2D metals. From the surface potential maps of QFEG, 2D Ag, 2D Ga, and 2D In in Figure 1d, we were able to extract the Fermi level of graphene under the influence of different 2D metals as summarized in Figure 1e. The obtained graphene Fermi level energies are −4.63, −4.56, −4.55, and −4.54 eV for QFEG, 2D Ag, 2D Ga, and 2D In, respectively. Compared with undoped graphene in the standard highly oriented pyrolytic graphite (HOPG), the Fermi level of graphene in QFEG is lowered by 0.03 eV due to the hole doping from hydrogen intercalation, while 2D metals all result in an upshift of graphene Fermi level, indicating electron injection from the metal to graphene. The observed shift of graphene Fermi level is in agreement with previous reports on angle-resolved photoemission spectroscopy (ARPES) measurements, where the Fermi levels of graphene on 2D Ga and QFEG were 0.2 eV above and 0.1 eV below the Dirac point, respectively.[30] The softened 2D peak of graphene after 2D metal intercalation compared to that after hydrogen intercalation also indicates that the graphene is electron doped on 2D metals (Figure S5).[9,31] These findings collectively confirm the Fermi level shift of graphene, which alters the band alignment of the molecules and graphene, ultimately modifying the GERS effect.

The different Fermi level tuning of graphene depending on the type of 2D metals is consistent with the work function of the bulk metals, for silver, gallium, and indium are reported to be 4.26, 4.20, and 4.12 eV, respectively.[32] Metals with higher Fermi levels, such as indium, are expected to donate more electrons to graphene and contribute to a stronger electron doping. It is also worth noting that the KPFM measures the Fermi level of graphene instead of the metal since KPFM is a surface sensitive technique. Furthermore, the trend of electron doping level for these 2D metals is in agreement with the electronegativity of the metals, in that metals having lower electronegativity tend to have weaker binding of electrons (In (1.78) < Ga (1.81) < Ag (1.93)).

GERS Modulated by the Graphene Fermi Level. The CuPc molecule was employed as a probe to study the Fermi level modulated GERS effect arising from the 2D metal intercalation. CuPc molecules were deposited on 2D metals through high vacuum thermal evaporation, forming a CuPc/graphene/metal/SiC heterostructure (Figure S4b). Figure 2 shows the Raman enhancement of CuPc on QFEG and 2D metals (2D Ag, 2D Ga, and 2D In). CuPc has Raman modes at 1147 cm^{-1}, 1344 cm^{-1}, 1455 cm^{-1}, and 1532 cm^{-1} under the 633 nm laser excitation as shown in Figure 2a. The Raman intensity of CuPc on these substrates was found to be strongly enhanced when compared with that on bare SiC (Figure S6), thus indicating a significant GERS effect. The enhancement factor (EF) of around 30 for CuPc Raman modes at around 1530 cm^{-1} on 2D metals is comparable to that of exfoliated graphene previously reported,[8] suggesting that the Raman enhancement is entirely contributed by the graphene layer with a Fermi level modified by the presence of the 2D metals. To elucidate the modified GERS performance, the intensity of the characteristic Raman modes of CuPc on different substrates was analyzed by normalizing to the Raman intensity of CuPc on 2D Ga. A normalized Raman intensity larger than 1 corresponds to a better GERS performance of this substrate compared to 2D Ga. As shown in Figure 2b, QFEG exhibits

https://doi.org/10.1021/acsnano.3c12152
ACS Nano 2024, 18, 8876−8884

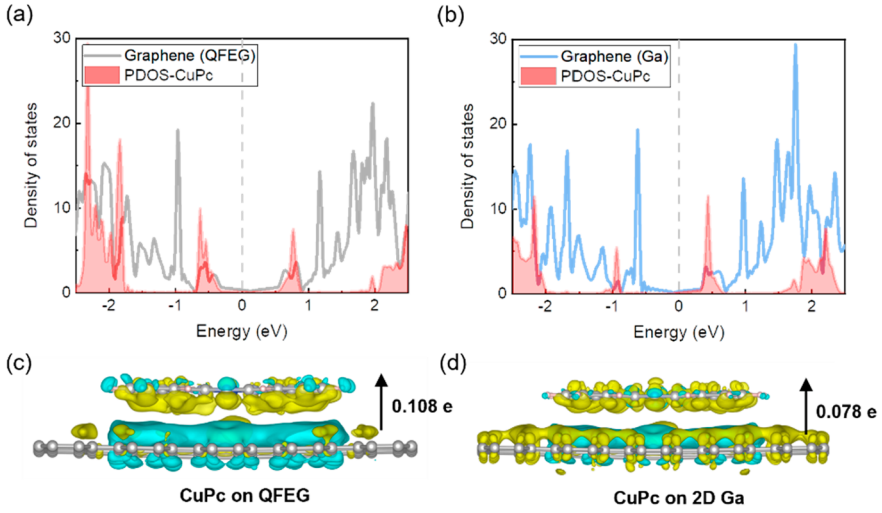

Figure 3. DOS and charge transfer of CuPc/graphene from DFT calculations. The calculated PDOS of CuPc (denoted by the filled curves) and graphene on QFEG (a) and 2D Ga (b). The vertical dashed line indicated the Fermi level of the system. (c,d) Side-view renderings of electron density difference isosurfaces for CuPc adsorbed onto QFEG and 2D Ga, respectively. Yellow color represents the electron accumulation, and blue color shows the electron depletion for the coupled structure compared to the individual component. The arrows represent the direction of charge transfer.

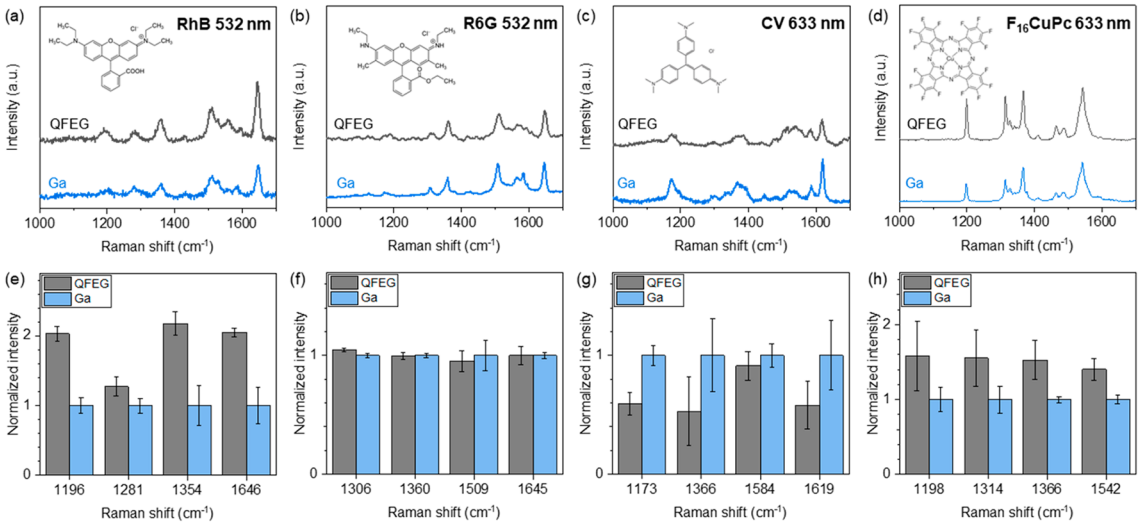

Figure 4. Raman enhancement of different molecules on QFEG and 2D Ga. Raman spectra of (a) RhB, (b) R6G, (c) CV, and (d) F_{16}CuPc on QFEG and 2D Ga. Normalized intensity of characteristic Raman modes of (e) RhB, (f) R6G, (g) CV, and (h) F_{16}CuPc.

better Raman enhancement for the CuPc Raman mode at 1147 cm^{-1}, in comparison with 2D metals. The Raman enhancement also depends on the type of metal intercalated under graphene, as 2D Ag shows a higher normalized Raman intensity than 2D Ga, which is again better than 2D In (2D Ag > 2D Ga > 2D In). In addition to the 1147 cm^{-1} mode, all vibrational modes of CuPc analyzed were found to show a similar dependence on the metal element, as the normalized Raman intensities decrease from 2D Ag to 2D Ga and to 2D In. The variation between different 2D metals is less pronounced potentially because of the phonon-assisted resonant scattering, where the phonon energy matches the energy difference between the laser and the HOMO−LUMO gap. The possible participation of phonon-assisted resonance is supported by the observation of a stronger Raman enhancement for higher-frequency phonons (Figure S7).

The variations of Raman enhancement among different 2D metals can be explained well by the band alignment for charge transfer between graphene and the molecules. Under the photoexcitation, a closer band alignment between the molecular orbits with the Fermi levels of graphene would enable a stronger hybridization and an enhanced charge transfer.[17] The HOMO and LUMO levels of the CuPc molecules have been extensively reported to be around −5.2 eV and −3.5 eV,[33] respectively. In such an energy configuration, as illustrated in Figure 2c,d, the charge transfer between the HOMO of CuPc and the Fermi level of graphene will be favored. Graphene with a lower Fermi energy will provide better hybridization of the wave function with the molecules and further improve charge transfer (Figure 2c). Consequently, the QFEG with the lowest Fermi energy exhibits the strongest Raman enhancement among the measured samples, while the 2D metals with higher Fermi

https://doi.org/10.1021/acsnano.3c12152
ACS Nano 2024, 18, 8876−8884

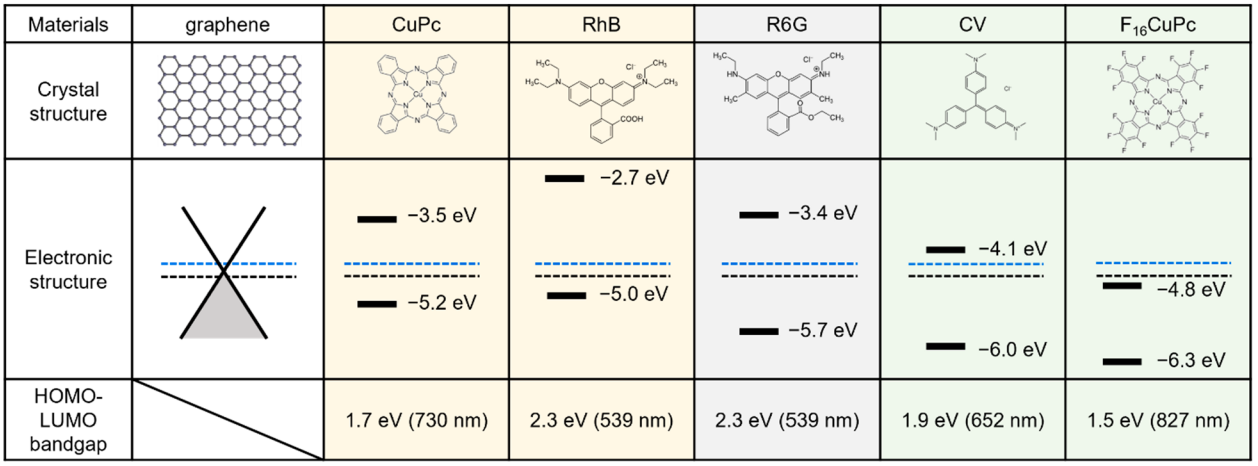

Figure 5. Molecular orbitals of different molecules and the band alignment with QFEG (gray dashed line) and 2D Ga (blue dashed line).

levels lead to weaker GERS enhancements as summarized by the Raman modes at 1147 cm^{-1}, 1344 cm^{-1}, and 1455 cm^{-1} to 1532 am^{-1} (Figure 2b).

We performed DFT calculations to investigate the coupling strength and charge transfer between CuPc and graphene with varying Fermi level tuning scenarios by comparing QFEG and 2D metals. The geometry of CuPc adsorption on graphene is shown in Figure S8a. The adsorption energies of CuPc on graphene in the presence of QFEG, 2D-Ag, 2D-Ga, and 2D-In substrates are −2.36, −2.30, −2.29, and −2.28 eV, respectively, thus indicating that QFEG results in better coupling affinity of CuPc/graphene when compared to the other substrates. The electronic density of states (DOS) of the CuPc/graphene clusters on these substrates was also obtained (Figure S8b) and the DOS projected on the adsorbed CuPc molecules (PDOS) and graphene are depicted in Figure 3, where the calculated molecular orbital of CuPc on the QFEG (Figure 3a) substrate has a better overlap with graphene compared to that on 2D Ga (Figure 3b) and other 2D metals (Figure S8c,d). This seems to allow more efficient charge transfer in the Raman scattering of CuPc on QFEG. Furthermore, the charge transfer analysis (shown in Figure 3c,d and Figure S8e,f) indicates that the electrons transferred from graphene to CuPc are 0.108*e* (QFEG), 0.084*e* (2D Ag), 0.078*e* (2D Ga), and 0.072*e* (2D In), respectively. The strongest interface dipole is formed between CuPc and graphene in QFEG. Consequently, the best GERS performance occurs for QFEG rather than the 2D metals. This can be attributed to the strongest adsorption energy and the most efficient charge transfer from the adsorbates to the substrates.

Molecular Selectivity Tuned by Band Alignment. To confirm that the influence of the Fermi-level-tuned GERS effect can be widely extended to other analyte molecules, we investigated the GERS performance of 2D metals for dye molecules with varied HOMO/LUMO energies, including RhB, R6G, CV, and F_{16}CuPc. As shown in Figure 4a−d, the Raman spectra obtained from these molecules on the QFEG and 2D Ga substrates were analyzed. The intensity of the characteristic Raman modes of the molecules on different substrates was again normalized to the intensity obtained on 2D Ga. The comparison between the enhancement from 2D Ga and QFEG shows that the GERS substrate plays an important role in determining the enhancement performance for each molecule. Similar to the case of CuPc, RhB exhibits stronger Raman modes on QFEG with a Raman intensity around twice those observed on 2D Ga (Figure 4e). This is consistent with the HOMO/LUMO energy of RhB, which is −2.7/−5.0 eV,[34] forming type II band alignment with graphene (Figure 5). The closer alignment of the RhB HOMO with the graphene Fermi level leads to a better hybridization of the wave function and charge transfer between graphene and the molecule, thus strongly contributing to the GERS effect.

In contrast, the modified graphene Fermi level in QFEG and 2D Ga is relatively centered between the HOMO/LUMO of R6G.[35] Therefore, the Fermi level tuning by 0.08 eV as confirmed by KPFM does not have a significant effect on the charge transfer probability, resulting in a similar normalized Raman intensity for 2D Ga and QFEG (Figure 4f). In terms of CV, it is notable that the graphene Fermi level is still situated between its HOMO/LUMO (−4.1 eV/−6.0 eV),[36,37] but the Fermi level is in close proximity to the LUMO rather than the HOMO. Herein, the process of charge transfer takes place between the LUMO of CV and the Fermi level of graphene. The higher graphene Fermi level in 2D Ga compared to the case in QFEG provides better energy matching, which contributes to a 60% enhancement of the Raman features of CV on 2D Ga when compared to QFEG (Figure 4g). Regarding F_{16}CuPc, it is noteworthy that its HOMO/LUMO levels lie below the modified graphene Fermi level of both QFEG and 2D Ga. Hence, the GERS arises from the charge transfer between the LUMO of F_{16}CuPc and the graphene Fermi level. As a consequence of this specific band alignment, QFEG again provides a better GERS effect for F_{16}CuPc compared to 2D Ga because of a better overlap between the Fermi level (−4.67 eV) and the LUMO (−4.8 eV).[38] Similar results were also observed for 2D Ag (Figure S9).

The different GERS performance depending on the doping of graphene ensures the molecular selectivity, as has been demonstrated for the above molecules. Based on the perturbation theory of Raman scattering and Fermi's Golden Rule,[39] the transition matrix element of the molecule increases when the disparity between the graphene Fermi level and the electronic levels of the molecule decreases, thereby resulting in a higher probability of electronic transition in the Raman scattering process. By deterministically modifying the Fermi level of graphene, we expect to achieve better energy level alignment in molecule−graphene systems, subsequently

https://doi.org/10.1021/acsnano.3c12152
ACS Nano 2024, 18, 8876−8884

leading to an even higher yield of electronic transition and an enhanced GERS effect. The precise tuning of the Fermi level by means of 2D metals would facilitate the development of high-specificity and precision sensors for a wide range of medical, environmental, and industrial applications.

CONCLUSIONS

In conclusion, we have demonstrated an innovative strategy of utilizing 2D metals to precisely and deterministically modulate the graphene Fermi level, thereby achieving an enhanced and selective GERS performance. The introduction of a few layers of metal atoms (2D metals) as chemical dopants beneath graphene creates a graphene/metal/SiC structure, enabling precise Fermi level tuning. This Fermi level modulation was verified by KPFM, which revealed a strong electron doping effect. Through the example of the CuPc molecules, our work illustrated how fine-tuning of the Fermi level resulted in an improved GERS enhancement. By aligning the graphene Fermi level closer to the HOMO of CuPc, we achieved a significant improvement in Raman enhancement. The efficacy of our approach was confirmed by DFT calculations, which support the enhanced charge transfer between CuPc and graphene and the favored adsorption of the molecules in this optimized Fermi level alignment. Our exploration extended beyond CuPc and considered diverse molecules such as R6G, RhB, CV, and F_{16}CuPc. This comprehensive study clearly demonstrated that Fermi level tuning mediated by 2D metals can be tailored to achieve molecular selectivity in GERS.

This work explores the capacity to manipulate energy levels in 2D materials through strategic Fermi level tuning, thus inspiring further research in the design and optimization of GERS substrates for a wide range of molecular detection and sensing applications. The fine control and modulation of the Fermi level through 2D metals not only enhance the GERS performance but also contribute to the selectivity and precision of sensing applications. By harnessing the potential of 2D metals and their impact on the interaction between graphene and analyte molecules, our findings are expected to have significant implications in the development of high-sensitivity, high-specificity, and reliable sensors for medical, environmental, and industrial applications.

METHODS

2D Metal Synthesis. The epitaxial graphene was first synthesized via high-temperature Si sublimation of SiC. The QFEG was obtained then after 12 h of annealing at 450 °C under 100 Torr of hydrogen. A thermal vaporization-based method was employed to intercalate 2D Ag, 2D Ga, and 2D In at the interface of epitaxial graphene/SiC. In order to introduce defects in the graphene layers, we exposed it to an O_2/He plasma. Next, we placed 30−60 mg of Ag, Ga, or In metal, along with the defective graphene sample, in an alumina crucible within a Lindberg/Blue M Mini Mite tube furnace equipped with a 1 in. outer diameter quartz tube. The furnace was then heated to 600−800 °C under 300 Torr of argon and 50 sccm continuous argon flow for 30 min, resulting in metal intercalation at the epitaxial graphene/SiC interface. The defects in epitaxial graphene were recovered after interaction, as shown in Figure S10.

Transmission Electron Microscopy. High angle annular dark-field scanning transmission electron microscopy (HAADF-STEM) imaging was performed on an FEI Titan^3 G2 S/TEM operating at an accelerating voltage of 80 kV, with a probe convergence angle of 30 mrad, a probe current of 70 pA, and ADF detector angles of 42−244 mrad.

Kelvin Probe Force Microscopy. KPFM measurement was conducted using the Bruker Dimension Icon system with an aluminum-coated silicon tip, which was calibrated on a highly oriented pyrolytic graphite (HOPG) surface (work function known as 4.6 eV) following the equation: $\Phi_s = \Phi_t - e\Delta V_{CPD}$, where Φ_s and Φ_t are the work function of the sample and the KPFM tip, respectively. The ΔV_{CPD} is the contact potential difference between the probe tip and the material surfaces. The Fermi level variation of the graphene with different intercalation could be calculated based on the work function of the tip, as the work function is defined as the energy difference between the Fermi level and vacuum level (usually set as 0 eV).

X-ray Photoelectron Spectroscopy. The XPS measurement was performed using a Physical Electronics VersaProbe III instrument equipped with a monochromatic Al Kα X-ray source ($h\nu$ = 1486.6 eV) and a concentric hemispherical analyzer. Charge neutralization was performed using both low energy electrons (<5 eV) and argon ions. The binding energy axis was calibrated using sputter cleaned Cu (Cu 2p3/2 = 932.62 eV, Cu 3p3/2 = 75.1 eV) and Au foils (Au 4f7/2 = 83.96 eV). Peaks were charged referenced to the sp^2 band in the carbon 1s spectra at 284.5 eV. Measurements were made at a takeoff angle of 45° with respect to the sample surface plane. This resulted in a typical sampling depth of 3−6 nm (95% of the signal originated from this depth or shallower). Quantification was done using instrumental relative sensitivity factors (RSFs) that account for the X-ray cross section and inelastic mean free path of the electrons. The analysis size was ∼200 μm in diameter.

Molecule Deposition. CuPc and F_{16}CuPc molecules were deposited on the substrate by a standard thermal evaporator (Angstrom Engineering) with the pressure at about 5×10^{-5} Pa. The evaporation thickness of the molecule was around 3 Å and was monitored using a quartz crystal monitor. RhB, R6G, and CV molecules were deposited on QFEG and 2D metal substrates by drop-casting for Raman measurement and analysis. First, a mild plasma treatment of 60 s was utilized to increase the hydrophilicity of the substrates using an ozone plasma cleaner. Then, a small droplet around 5 μL of the dye solution was placed onto the substrate using a micropipette. The droplet was allowed to dry under ambient conditions. Finally, the substrates were gently rinsed with deionized water to remove any unbound molecules.

Raman Spectroscopy. The Horiba LabRam HR evolution confocal Raman system with a 532 nm DPSS laser line and a 633 nm He−Ne laser line was used to conduct Raman measurements. The sample was focused by a 100× objective with the excitation laser power of approximately 1 mW. The typical exposure time is 5 s, and the accumulation time is 2. All spectra were averaged after at least three measurements on different spots of the samples. The Raman peaks were fitted using a Lorenz-Gaussian function with LabSpec software to determine the Raman shifts and intensity.

First-Principle Calculations. All DFT calculations were performed using the Vienna ab initio simulation package (VASP) code with the projector augmented wave (PAW) method.[40,41] We used the Perdew−Burke−Ernzerhof (PBE) functional to describe the exchange-correlation interactions.[42] The van der Waals (vdW) interaction was handled using the DFT-D3 method with the semiempirical Grimme parameters.[43,44] The kinetic energy cutoff for the plane-wave expansion was set to 450 eV. The convergence energy and force for the geometrical optimization were set to 10^{-5} eV and 0.01 eV/Å, respectively. The Brillouin zone was sampled through a 2 × 2 × 2 k-point mesh with a vacuum layer of 20 Å. The adsorption energy for CuPc adsorbed on the sample substrate was calculated using $E_{ads} = E_{tot} - E_{sam} - E_{CuPc}$, where E_{sam}, E_{CuPc}, and E_{tot} are the energies of the sample substrate, CuPc, and the CuPc/sample system, respectively.

ASSOCIATED CONTENT

Supporting Information

The Supporting Information is available free of charge at https://pubs.acs.org/doi/10.1021/acsnano.3c12152.

SEM image of 2D Ag; AFM images of 2D Ag, 2D Ga, 2D In, QFEG, EG, and HOPG; XPS of C 1s for as-

https://doi.org/10.1021/acsnano.3c12152
ACS Nano 2024, 18, 8876−8884

grown QFEG, 2D Ag, 2D Ga, and 2D In; schematic illustration of EG, QFEG, and the CuPC/graphene/2D Ag/SiC heterostructure; Raman spectrum of QFEG, 2D Ag, 2D Ga, and 2D In; Raman enhancement of CuPc on 2D Ag; Raman intensity normalized by the Raman mode at 1530 cm^{-1} for different Raman modes of CuPc under 633 nm laser excitation; adsorption structure and charge transfer of CuPc/graphene from DFT calculations; Raman enhancement of different molecules on QFEG, 2D Ga, and 2D Ag; Raman spectrum of graphene before and after intercalation of metal atoms (PDF)

AUTHOR INFORMATION

Corresponding Authors

Wei Hu − *School of Chemistry and Chemical Engineering, Qilu University of Technology (Shandong Academy of Sciences), Jinan, Shandong 250353, People's Republic of China;* orcid.org/0000-0002-7467-4783; Email: weihu@qlu.edu.cn

Shengxi Huang − *Department of Electrical and Computer Engineering, Rice University, Houston, Texas 77005, United States;* orcid.org/0000-0002-3618-9074; Email: shengxi.huang@rice.edu

Mauricio Terrones − *Department of Physics, The Pennsylvania State University, University Park, Pennsylvania 16802, United States; Department of Materials Science and Engineering, Department of Chemistry, Two-Dimensional Crystal Consortium, and Center for Two-Dimensional and Layered Materials, The Pennsylvania State University, University Park, Pennsylvania 16802, United States;* orcid.org/0000-0003-0010-2851; Email: mut11@psu.edu

Authors

Na Zhang − *Department of Physics, The Pennsylvania State University, University Park, Pennsylvania 16802, United States;* orcid.org/0000-0002-0682-564X

Kunyan Zhang − *Department of Electrical and Computer Engineering, Rice University, Houston, Texas 77005, United States*

Min Zou − *School of Chemistry and Chemical Engineering, Qilu University of Technology (Shandong Academy of Sciences), Jinan, Shandong 250353, People's Republic of China*

Rinu Abraham Maniyara − *Department of Materials Science and Engineering, The Pennsylvania State University, University Park, Pennsylvania 16802, United States;* orcid.org/0000-0002-8380-7752

Timothy Andrew Bowen − *Department of Materials Science and Engineering, The Pennsylvania State University, University Park, Pennsylvania 16802, United States*

Jonathon Ray Schrecengost − *Department of Electrical Engineering, The Pennsylvania State University, University Park, Pennsylvania 16802, United States;* orcid.org/0009-0008-5093-5839

Arpit Jain − *Department of Materials Science and Engineering, The Pennsylvania State University, University Park, Pennsylvania 16802, United States*

Da Zhou − *Department of Physics, The Pennsylvania State University, University Park, Pennsylvania 16802, United States;* orcid.org/0000-0002-7189-5222

Chengye Dong − *Department of Materials Science and Engineering, The Pennsylvania State University, University Park, Pennsylvania 16802, United States*

Zhuohang Yu − *Department of Materials Science and Engineering, The Pennsylvania State University, University Park, Pennsylvania 16802, United States*

He Liu − *Department of Chemistry, The Pennsylvania State University, University Park, Pennsylvania 16802, United States*

Noel C. Giebink − *Department of Electrical Engineering, The Pennsylvania State University, University Park, Pennsylvania 16802, United States; Department of Electrical Engineering and Computer Science, University of Michigan, Ann Arbor, Michigan 48109, United States;* orcid.org/0000-0002-3798-5830

Joshua A. Robinson − *Department of Materials Science and Engineering, Two-Dimensional Crystal Consortium, and Center for Two-Dimensional and Layered Materials, The Pennsylvania State University, University Park, Pennsylvania 16802, United States;* orcid.org/0000-0002-1513-7187

Complete contact information is available at: https://pubs.acs.org/10.1021/acsnano.3c12152

Author Contributions

¶These authors contributed equally.

Author Contributions

S.H. and M.T. proposed and supervised the project. N.Z. and K.Z. conducted the sample preparation and spectroscopy measurement. M.Z. and W.H. contributed to the theoretical calculation. R.A.M., T.A.B., C.D., A.J., and J.A.R. contributed to the synthesis of 2D metals. J.R.S., A.J., and N.C.G. contributed to the thermal evaporation for molecule deposition. D.Z. and N.Z. contributed to the KPFM measurement. Z.Y. and H.L. contributed to the XPS data analysis. N.Z. and K.Z. performed the analysis of the data and wrote the manuscript with the input from all coauthors. All of the authors discussed the results and revised the paper.

Notes

The authors declare no competing financial interest.

ACKNOWLEDGMENTS

The authors thank J. Shallenberger for XPS measurement and K. Wang for TEM characterization. This work was supported by National Science Foundation (NSF) under DMR-1420620 and DMR-2011839 through the Penn State MRSEC−Center for Nanoscale Science, Atomically Thin Multifunctional Coatings (ATOMIC) Award 1540018 through the Industry−University Cooperative Research Centers (IUCRC), ECCS-2230400, ECCS-1943895, and ECCS-2246564, as well as Welch Foundation (Award No. C-2144).

REFERENCES

(1) Langer, J.; Jimenez De Aberasturi, D.; Aizpurua, J.; Alvarez-Puebla, R. A.; Auguié, B.; Baumberg, J. J.; Bazan, G. C.; Bell, S. E. J.; Boisen, A.; Brolo, A. G.; Choo, J.; Cialla-May, D.; Deckert, V.; Fabris, L.; Faulds, K.; García De Abajo, F. J.; Goodacre, R.; Graham, D.; Haes, A. J.; Haynes, C. L.; Huck, C.; Itoh, T.; Käll, M.; Kneipp, J.; Kotov, N. A.; Kuang, H.; Le Ru, E. C.; Lee, H. K.; Li, J.-F.; Ling, X. Y.; Maier, S. A.; Mayerhöfer, T.; Moskovits, M.; Murakoshi, K.; Nam, J.-M.; Nie, S.; Ozaki, Y.; Pastoriza-Santos, I.; Perez-Juste, J.; Popp, J.; Pucci, A.; Reich, S.; Ren, B.; Schatz, G. C.; Shegai, T.; Schlücker, S.; Tay, L.-L.; Thomas, K. G.; Tian, Z.-Q.; Van Duyne, R. P.; Vo-Dinh, T.; Wang, Y.; Willets, K. A.; Xu, C.; Xu, H.; Xu, Y.; Yamamoto, Y. S.;

Zhao, B.; Liz-Marzán, L. M. Present and Future of Surface-Enhanced Raman Scattering. *ACS Nano* **2020**, *14* (1), 28−117.
(2) Schlucker, S. Surface-Enhanced Raman Spectroscopy: Concepts and Chemical Applications. *Angew. Chem., Int. Ed.* **2014**, *53* (19), 4756−4795.
(3) Zhang, K.; Wang, Z.; Liu, H.; Perea-López, N.; Ranasinghe, J. C.; Bepete, G.; Minns, A. M.; Rossi, R. M.; Lindner, S. E.; Huang, S. X.; Terrones, M.; Huang, S. Understanding the Excitation Wavelength Dependence and Thermal Stability of the SARS-CoV-2 Receptor-Binding Domain Using Surface-Enhanced Raman Scattering and Machine Learning. *ACS Photonics* **2022**, *9* (9), 2963−2972.
(4) Xu, W.; Mao, N.; Zhang, J. Graphene: A Platform for Surface-Enhanced Raman Spectroscopy. *Small* **2013**, *9* (8), 1206−1224.
(5) Zong, C.; Xu, M. X.; Xu, L. J.; Wei, T.; Ma, X.; Zheng, X. S.; Hu, R.; Ren, B. Surface-Enhanced Raman Spectroscopy for Bioanalysis: Reliability and Challenges. *Chem. Rev.* **2018**, *118* (10), 4946−4980.
(6) Zhang, E.; Xing, Z.; Wan, D.; Gao, H.; Han, Y.; Gao, Y.; Hu, H.; Cheng, Z.; Liu, T. Surface-enhanced Raman spectroscopy chips based on two-dimensional materials beyond graphene. *Journal of Semiconductors* **2021**, *42*, 051001.
(7) Tian, H.; Zhang, N.; Tong, L.; Zhang, J. In Situ Quantitative Graphene-Based Surface-Enhanced Raman Spectroscopy. *Small Methods* **2017**, *1* (6), 1700126.
(8) Ling, X.; Xie, L.; Fang, Y.; Xu, H.; Zhang, H.; Kong, J.; Dresselhaus, M. S.; Zhang, J.; Liu, Z. Can Graphene be used as a Substrate for Raman Enhancement? *Nano Lett.* **2010**, *10* (2), 553−561.
(9) Zhang, S.; Zhang, N.; Zhao, Y.; Cheng, T.; Li, X.; Feng, R.; Xu, H.; Liu, Z.; Zhang, J.; Tong, L. Spotting the differences in two-dimensional materials − the Raman scattering perspective. *Chem. Soc. Rev.* **2018**, *47* (9), 3217−3240.
(10) Ling, X.; Huang, S.; Deng, S.; Mao, N.; Kong, J.; Dresselhaus, M. S.; Zhang, J. Lighting Up the Raman Signal of Molecules in the Vicinity of Graphene Related Materials. *Acc. Chem. Res.* **2015**, *48* (7), 1862−1870.
(11) Kitadai, H.; Wang, X.; Mao, N.; Huang, S.; Ling, X. Enhanced Raman Scattering on Nine 2D van der Waals Materials. *J. Phys. Chem. Lett.* **2019**, *10* (11), 3043−3050.
(12) Zhang, N.; Tong, L.; Zhang, J. Graphene-Based Enhanced Raman Scattering toward Analytical Applications. *Chem. Mater.* **2016**, *28* (18), 6426−6435.
(13) Lin, Y.-C.; Torsi, R.; Younas, R.; Hinkle, C. L.; Rigosi, A. F.; Hill, H. M.; Zhang, K.; Huang, S.; Shuck, C. E.; Chen, C.; Lin, Y.-H.; Maldonado-Lopez, D.; Mendoza-Cortes, J. L.; Ferrier, J.; Kar, S.; Nayir, N.; Rajabpour, S.; van Duin, A. C. T.; Liu, X.; Jariwala, D.; Jiang, J.; Shi, J.; Mortelmans, W.; Jaramillo, R.; Lopes, J. M. J.; Engel-Herbert, R.; Trofe, A.; Ignatova, T.; Lee, S. H.; Mao, Z.; Damian, L.; Wang, Y.; Steves, M. A.; Knappenberger, K. L., Jr.; Wang, Z.; Law, S.; Bepete, G.; Zhou, D.; Lin, J.-X.; Scheurer, M. S.; Li, J.; Wang, P.; Yu, G.; Wu, S.; Akinwande, D.; Redwing, J. M.; Terrones, M.; Robinson, J. A. Recent Advances in 2D Material Theory, Synthesis, Properties, and Applications. *ACS Nano* **2023**, *17* (11), 9694−9747.
(14) Wang, Z.; Ye, J.; Zhang, K.; Ding, L.; Granzier-Nakajima, T.; Ranasinghe, J. C.; Xue, Y.; Sharma, S.; Biase, I.; Terrones, M.; Choi, S. H.; Ran, C.; Tanzi, R. E.; Huang, S. X.; Zhang, C.; Huang, S. Rapid Biomarker Screening of Alzheimer's Disease by Interpretable Machine Learning and Graphene-Assisted Raman Spectroscopy. *ACS Nano* **2022**, *16* (4), 6426−6436.
(15) Zhang, N.; Lin, J.; Hu, W.; Zhang, S.; Liang, L.; Wang, R.; Luo, X.; Luo, Y.; Qiu, X.; Zhang, J.; Tong, L. Bifacial Raman Enhancement on Monolayer Two-Dimensional Materials. *Nano Lett.* **2019**, *19* (2), 1124−1130.
(16) Ling, X.; Fang, W.; Lee, Y.-H.; Araujo, P. T.; Zhang, X.; Rodriguez-Nieva, J. F.; Lin, Y.; Zhang, J.; Kong, J.; Dresselhaus, M. S. Raman Enhancement Effect on Two-Dimensional Layered Materials: Graphene, h-BN and MoS_2. *Nano Lett.* **2014**, *14* (6), 3033−3040.
(17) Huang, S.; Ling, X.; Liang, L.; Song, Y.; Fang, W.; Zhang, J.; Kong, J.; Meunier, V.; Dresselhaus, M. S. Molecular Selectivity of Graphene-Enhanced Raman Scattering. *Nano Lett.* **2015**, *15* (5), 2892−2901.
(18) Singh, A. K.; Singh, R. S.; Singh, A. K. Recent Developments in Chemical Doping of Graphene using Experimental Approaches and Its Applications. *Adv. Eng. Mater.* **2022**, *24* (11), 2200259.
(19) Hao, Q.; Morton, S. M.; Wang, B.; Zhao, Y.; Jensen, L.; Jun Huang, T. Tuning surface-enhanced Raman scattering from graphene substrates using the electric field effect and chemical doping. *Appl. Phys. Lett.* **2013**, *102* (1), 011102.
(20) Xu, H.; Xie, L.; Zhang, H.; Zhang, J. Effect of Graphene Fermi Level on the Raman Scattering Intensity of Molecules on Graphene. *ACS Nano* **2011**, *5* (7), 5338−5344.
(21) Soo Park, C.; Zhao, Y.; Lee, J.-H.; Whang, D.; Shon, Y.; Song, Y.-H.; Jin Lee, C. Tunable bandgap of a single layer graphene doped by the manganese oxide using the electrochemical doping. *Appl. Phys. Lett.* **2013**, *102* (3), 032106.
(22) Luo, Z.; Pinto, N. J.; Davila, Y.; Charlie Johnson, A. T. Controlled doping of graphene using ultraviolet irradiation. *Appl. Phys. Lett.* **2012**, *100* (25), 253108.
(23) Feng, S.; dos Santos, M. C.; Carvalho, B. R.; Lv, R.; Li, Q.; Fujisawa, K.; Elías, A. L.; Lei, Y.; Perea-López, N.; Endo, M.; Pan, M.; Pimenta, M. A.; Terrones, M. Ultrasensitive molecular sensor using N-doped graphene through enhanced Raman scattering. *Science Advances* **2016**, *2* (7), No. e1600322.
(24) Wei, D.; Liu, Y.; Wang, Y.; Zhang, H.; Huang, L.; Yu, G. Synthesis of N-Doped Graphene by Chemical Vapor Deposition and Its Electrical Properties. *Nano Lett.* **2009**, *9* (5), 1752−1758.
(25) Ryu, S.; Liu, L.; Berciaud, S.; Yu, Y.-J.; Liu, H.; Kim, P.; Flynn, G. W.; Brus, L. E. Atmospheric Oxygen Binding and Hole Doping in Deformed Graphene on a SiO2 Substrate. *Nano Lett.* **2010**, *10* (12), 4944−4951.
(26) Criado, A.; Melchionna, M.; Marchesan, S.; Prato, M. The Covalent Functionalization of Graphene on Substrates. *Angew. Chem., Int. Ed.* **2015**, *54* (37), 10734−10750.
(27) Wang, X. W.; Sun, G. Z.; Routh, P.; Kim, D. H.; Huang, W.; Chen, P. Heteroatom-doped graphene materials: syntheses, properties and applications. *Chem. Soc. Rev.* **2014**, *43* (20), 7067−7098.
(28) Ashraf, A.; Wu, Y.; Wang, M. C.; Yong, K.; Sun, T.; Jing, Y.; Haasch, R. T.; Aluru, N. R.; Nam, S. Doping-Induced Tunable Wettability and Adhesion of Graphene. *Nano Lett.* **2016**, *16* (7), 4708−4712.
(29) Nisi, K.; Subramanian, S.; He, W.; Ulman, K. A.; El-Sherif, H.; Sigger, F.; Lassaunière, M.; Wetherington, M. T.; Briggs, N.; Gray, J.; Holleitner, A. W.; Bassim, N.; Quek, S. Y.; Robinson, J. A.; Wurstbauer, U. Light−Matter Interaction in Quantum Confined 2D Polar Metals. *Adv. Funct. Mater.* **2021**, *31* (4), 2005977.
(30) Briggs, N.; Bersch, B.; Wang, Y.; Jiang, J.; Koch, R. J.; Nayir, N.; Wang, K.; Kolmer, M.; Ko, W.; De La Fuente Duran, A.; Subramanian, S.; Dong, C.; Shallenberger, J.; Fu, M.; Zou, Q.; Chuang, Y.-W.; Gai, Z.; Li, A.-P.; Bostwick, A.; Jozwiak, C.; Chang, C.-Z.; Rotenberg, E.; Zhu, J.; Van Duin, A. C. T.; Crespi, V.; Robinson, J. A. Atomically thin half-van der Waals metals enabled by confinement heteroepitaxy. *Nat. Mater.* **2020**, *19* (6), 637−643.
(31) Das, A.; Pisana, S.; Chakraborty, B.; Piscanec, S.; Saha, S. K.; Waghmare, U. V.; Novoselov, K. S.; Krishnamurthy, H. R.; Geim, A. K.; Ferrari, A. C.; Sood, A. K. Monitoring dopants by Raman scattering in an electrochemically top-gated graphene transistor. *Nat. Nanotechnol.* **2008**, *3* (4), 210−215.
(32) Michaelson, H. B. The work function of the elements and its periodicity. *J. Appl. Phys.* **1977**, *48* (11), 4729−4733.
(33) Chu, C.-W.; Shrotriya, V.; Li, G.; Yang, Y. Tuning acceptor energy level for efficient charge collection in copper-phthalocyanine-based organic solar cells. *Appl. Phys. Lett.* **2006**, *88* (15), DOI: 10.1063/1.2194207.
(34) Tian, H.; Zhang, N.; Zhang, J.; Tong, L. Exploring quantification in a mixture using graphene-based surface-enhanced Raman spectroscopy. *Applied Materials Today* **2019**, *15*, 288−293.
(35) Zhang, Y.; Shi, Y.; Wu, M.; Zhang, K.; Man, B.; Liu, M. Synthesis and surface-enhanced Raman scattering of ultrathin SnSe2

https://doi.org/10.1021/acsnano.3c12152
ACS Nano 2024, 18, 8876−8884

nanoflakes by chemical vapor deposition. *Nanomaterials* **2018**, *8* (7), 515.
(36) Zhao, H.; Zhang, Y.; Li, G.; Tian, F.; Tang, H.; Chen, R. Rhodamine B-sensitized BiOCl hierarchical nanostructure for methyl orange photodegradation. *RSC Adv.* **2016**, *6* (10), 7772−7779.
(37) Cañamares, M. V.; Chenal, C.; Birke, R. L.; Lombardi, J. R. DFT, SERS, and Single-Molecule SERS of Crystal Violet. *J. Phys. Chem. C* **2008**, *112* (51), 20295−20300.
(38) Shen, C.; Kahn, A.; Schwartz, J. Role of metal−molecule chemistry and interdiffusion on the electrical properties of an organic interface: The Al−F16CuPc case. *J. Appl. Phys.* **2001**, *90* (12), 6236−6242.
(39) Barros, E. B.; Dresselhaus, M. S. Theory of Raman enhancement by two-dimensional materials: Applications for graphene-enhanced Raman spectroscopy. *Phys. Rev. B* **2014**, *90* (3), 035443.
(40) Kresse, G.; Furthmüller, J. Efficient iterative schemes for ab initio total-energy calculations using a plane-wave basis set. *Phys. Rev. B* **1996**, *54* (16), 11169−11186.
(41) Blöchl, P. E. Projector augmented-wave method. *Phys. Rev. B* **1994**, *50* (24), 17953−17979.
(42) Perdew, J. P.; Burke, K.; Ernzerhof, M. Generalized Gradient Approximation Made Simple. *Phys. Rev. Lett.* **1996**, *77* (18), 3865−3868.
(43) Grimme, S.; Antony, J.; Ehrlich, S.; Krieg, H. A consistent and accurate ab initio parametrization of density functional dispersion correction (DFT-D) for the 94 elements H-Pu. *J. Chem. Phys.* **2010**, *132* (15), DOI: 10.1063/1.3382344.
(44) Grimme, S. Semiempirical GGA-type density functional constructed with a long-range dispersion correction. *J. Comput. Chem.* **2006**, *27* (15), 1787−1799.

https://doi.org/10.1021/acsnano.3c12152
ACS Nano 2024, 18, 8876−8884